10.5 AUTOMATED ESTIMATION OF WIND VECTORS FROM SAR

Christopher C. Wackerman[1], William G. Pichel[2], Pablo Clemente-Colòn[2]
[1] Veridian Systems Division, Ann Arbor Michigan
[2] NOAA/NESDIS, Camp Springs, Maryland

1. INTRODUCTION AND BACKGROUND

Satellite-based Synthetic Aperture Radar (SAR) sensors provide high resolution (12 to 100 meters) images of the earth's surface day or night and during most weather because they are active sensors operating in the microwave wavelengths (usually 3 to 20 centimeters). This makes them a potentially highly useful device for monitoring the earth, so much research has been done to determine the range of geophysical parameters that can be accurately estimated from SAR images. In particular, extracting environmental information from SAR images over the ocean has been an area of research for many years, and multiple approaches have been developed for characterizing a range of ocean parameters such as waves, winds, surf and currents. The work in this paper focuses on the use of SAR images to estimate wind vectors over the ocean and in coastal waters, and in particular to develop an operational and automated approach. If proved reliable, SAR images may be the only way to provide high spatial resolution wind vectors in coastal regions.

Almost all of these approaches to extract environmentally information from SAR images over the ocean are based on a standard theory for how a SAR images the ocean. This theory, often referred to as Bragg scattering (see Wright (1968) and Valenzuela (1978)) assumes that the variations in the SAR image brightness (or intensity) are proportional to the amplitude of ocean surface waves that are resonance to the electromagnetic wavelength of the SAR sensor. These resonant ocean waves will have a wavenumber k_B (where $k = 2\pi/\lambda$ and λ is the wave length of the wave) such that $k_B = 2k_{EM}\sin[\theta]$ where k_{EM} is the wavenumber of the electromagnetic wavelength and θ is the incidence angle of the sensor. In addition, these resonant waves need to be propagating either directly toward or away from the sensor. Thus the SAR is only observing very small-scale waves that are propagating in very specific directions. However, these small-scale waves are highly responsive to the local wind. As the local wind speed increases the amplitudes of these waves increase and thus the SAR image brightness increases. This phenomena forms the backbone of wind retrieval from SAR since it implies that the mean SAR image brightness (or radar cross section (RCS) as it is referred to when the image is absolutely calibrated) can be related to the local wind speed and direction. Note that wind direction (relative to the direction the sensor is looking) is very important because the amplitude of the small-scale waves will change significantly according to their propagation direction with respect to the local wind. This means the SAR image RCS will also change as the SAR look direction changes even though the wind speed stays constant since the RCS is proportional to the amplitude of the waves it observes.

Much work has been done to determine how to estimate wind vectors from SAR imagery based on this theory. The general approach is shown in Figure 1. It assumes a model that predicts the RCS given wind speed and direction. The procedure is to estimate the local RCS from the SAR image, estimate wind direction either from the SAR image or from some other source (most often from satellite-based scatterometers or from atmospheric models) then find the wind speed that reproduces the observed RCS.

What differentiates the various approaches are the RCS model used and the manner to estimate wind direction. For the European ERS-1/2 SAR sensors, which operate in VV polarization, the RCS model comes from validated scatterometer models (Vachon and Dobson (1996); Wackerman et al. (1996); Fetterer et al. (1998); Lehner et al. (1998); Lehner et al. (2000)). For the Canadian RADARSAT-1 SAR sensor, which operates in HH polarization, no such validated models exist so two approaches have been tried. The first is to derive an empirical modification to the VV models to convert them to HH polarization (Horstmann et al. (2000a); Horstmann et al. (2000b); Thompson and Beal (2000); Vachon and Dobson (2000); Horstmann et al. (2002); Monaldo et al. (2001)). The second approach is to derive analytical models directly for HH polarization (Wackerman et al. (2002)).

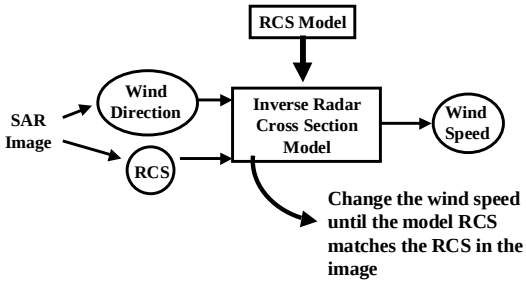

Figure 1: General approach to wind vector estimation using a SAR image.

Various approaches have also been developed for estimating the wind direction. One class of approaches estimates wind direction from the SAR image itself by noting that there are features in the imagery that tend to be aligned with the local wind. These can be wind rows, elongated convective cells, or surfactants on the ocean surface. These directions can be estimated in the spectral domain via Fourier transforms (Gerling (1986); Vachon and Dobson (1996); Wackerman et al. (1996); Fetterer et al. (1998); Lehner et al., (1998); Horstmann et al. (2000a); Horstmann et al. (2000b); Vachon and Dobson (2000)) or in the image domain via gradient estimators (Horstmann et al., 2002) or wavelet analysis (Du et al. (2002); Fichaux and Ranchin (2002)). The advantage of this class of approaches is that they generate the full wind vector solely from the SAR image without reference to any other data. The disadvantages are that the resulting wind directions have a 180° ambiguity (since from a single SAR image the feature alignment is ambiguous with respect to ±180°) and the features that are being used may not always be present in the SAR image or aligned with the wind. The second class of approaches utilize either simultaneous satellite-based scatterometer observations or atmospheric models to derive wind directions (Thompson and Beal (2000); Monaldo (2000); Monaldo et al. (2002)). This class of approaches has the advantage that a wind direction will always be available since it is derived separately from the SAR image. The disadvantage, particularly in the use of atmospheric models, is that the directions might not correspond accurately enough to the SAR image data.

Table 1 gives a summary of performance for these algorithms drawn from a sample of the published literature. Shown in Table 1 is the reference for the results and the sensor used (ERS = the ERS sensor, RAD = the RADARSAT sensor) with the number of images that went into the error estimation (although the Vachon and Dobson (2000) results are for the number of comparisons since the number of images was not described). Next is shown the root-mean-squared error (RMSE) for estimating wind direction from the SAR image. Note that all but the two indicated results used spectral approaches for estimating wind direction. Finally, the RMSE for wind speed is shown where three different wind direction are used. In the first column the direction derived from the SAR image is used, in the next column directions from a satellite-based scatterometer are used, in the last column directions from an atmospheric model are used. For the atmospheric models, the model name is indicated below the error. The performance of the various algorithms are very similar, and to derive a general sense of performance, the RMSE values are averaged over the different sources and shown on the bottom. General wind direction RMSE is 29 degrees and wind speed RMSE is around 2.2 m/s.

Source	**Sensor/# of images**	**Dir. RMSE**	**Speed RMSE (SAR dir.)**	**Speed RMSE (Scat. dir.)**	**Speed RMSE (model dir.)**
Wackerman et al. 1996	ERS/9	19°	1.2 m/s		
Fetterer et al. 1998	ERS/61	37°	2.0 m/s		
Vachon and Dobson 2000	ERS/65[1]	40°	1.9 m/s		
Vachon and Dobson 2000	RAD/77[1]	40°	2.4 m/s		
Horstmann et al. 2000a	RAD/4			2.7 m/s	
Horstmann et al. 2000a	RAD/9				2.9 m/s (HIRLAM)
Fichaux and Rachin 2002 (direction via wavlets)	ERS/1	16°			
Horstmann et al. 2002 (direction via gradient)	RAD/20	22°	3.5 m/s		
Monaldo et al. 2001	RAD/2862				2.0 m/s (NOGAPS)
This paper	RAD/32	32°	1.6 m/s		
Average Value		29°	2.1 m/s	2.4 m/s	2.3 m/s

[1] Number of comparisons, not number of images.

Table 1: Summary of wind vector estimation performance from various published papers.

The algorithm used in this paper will have the standard scatterometer model for VV RCS and the analytical model in Wackerman et al. (2002) for HH RCS, with wind directions estimated from the SAR image via spectral analysis. The interest of the authors is in moving this algorithm toward operational implementation. This means that: (1) the algorithm is completely automated; (2) it runs quickly; and (3) it can automatically remove "bad" wind direction estimates. This last component can be essentially since, as noted above, it is often the case that the SAR image does not contain features adequate for estimating wind direction. An operational algorithm needs to recognize this and replace the "bad" direction with an interpolated direction from its neighbors, or a default direction if the SAR image contains absolutely no wind direction information. In this paper we present initial results on our operational version of the wind vector algorithm and validate it with *in situ* buoy observations.

2. ALGORITHM DESCRIPTION

As mentioned above, Figure 1 shows the general flow of the algorithm. In developing the specific algorithm described in this section, we have attempted to make the algorithm operational in that it is totally automated and runs in a reasonable amount of time.

The first step is to estimate wind directions for a grid superimposed over the image. This is done by using the Fast Fourier Transform (FFT) to estimate the local spectrum of the image, then use the lower wavenumber portion of the spectrum to determine the direction of long-scale features in the image. SAR images are noisy however, so some smoothing of the spectrum is required. This is performed in two ways. First, multiple, overlapping, spectra are calculated for a given location and averaged. Second, the averaged spectrum is median filtered within a specified wavenumber annulus to reduce noise. In addition, the local image subset is flattened to reduce leakage from the DC component of the spectrum into the low wavenumber regime. The specific steps are as follows.

- The user specifies a local box size within which a wind direction will be estimated, a local FFT size (usually smaller than the box size), and the number and placement of the FFT's within the local box. For the results in this paper, four spectra were averaged for each wind direction where each spectra region had a 50% overlap with the neighboring spectrum.
- Each local box is flattened by applying a large average filter, then dividing by the filtered image.
- The FFT's are applied and the resulting spectra are averaged
- An annulus is applied to the spectrum to zero out any energy outside of a wavenumber region. For the results in this paper, the limits of the annulus were set to wave lengths of 3 km to 15 km.
- A 2D median filter is then applied to the spectrum. For the results in this paper the median filter was 3x3 samples.
- A 2D polynomial is fit to the resulting spectral samples and the direction through the origin which has the largest quadratic term (i.e. the widest extent) is determined. The wind direction is then assumed to be 90° from this direction.

Once all of the wind directions have been estimated for each grid point within the image, the directions are then spatially averaged with a weighted average where the weights are the normalized mean RCS values. This eliminates directions over dark regions in the image that are coming strictly from noise, and also imposes a smooth wind field across the entire image.

To handle land regions, a land mask is generated for each image from map data. If the middle of the local box is over land, that wind direction is not generated. If there are land pixels within the local box, they are set to the mean of the water samples within the box before the processes listed above are performed. This allows wind directions to be estimated close to shore as well as within water regions that may be behind land features or within large rivers. However, at least half the local box must be water samples or else it is ignored.

This process assumes that within the local box there is a feature in the SAR image that is aligned with the local wind. This is not always going to be true, so work is ongoing to determine whether a metric can be developed that will automatically flag a local box if it can not be used to generate an accurate wind direction. In that case it would be ignored as land regions are ignored. To date we have found that the shape of the 2D polynomial can provide some information, and in particular the ratio of the quadratic coefficients (minimum over maximum) for the two dimensions can characterize the shape of the low wavenumber energy. The ratio needs to be in the range [0.2,0.8] for the local box to generate accurate directions; if it is close to zero (or negative) or too large, that indicates that the low wavenumber spectral

region has anomalies that make it suspect. We are currently investigating additional metrics to use.

The resulting wind direction will have a 180° ambiguity since the procedure described below can not distinguish which direction along the feature the wind is blowing. Other image features may be able to resolve this ambiguity (such as wind shadowing), but to date we have not come up with an automated approach to do this. In the validation results below, the wind direction ambiguity is resolved by using whichever is closest to the *in situ* observations.

Once the wind directions are determined, we then estimate wind speed by inverting a RCS model. An analytical model was developed to handle the HH polarization imagery from RADARSAT and compared to other models in Wackerman et al. (2002). We showed that the analytical model had some improvements over other approaches, but was very similar to the model described in Thompson and Beal (2000). We are currently implementing the analytical model via a look-up table approach since the model itself is too computationally intensive to run for each wind estimate. RCS values are pre-calculated for a table of incidence angles, wind speeds, and sensor look directions (with respect to the local wind direction). A RCS value is then calculated for a given incidence angle, wind speed, and look direction using bi-linear interpolation within the table. For the table, wind speed is sampled every 1 m/s, incidence angle is sampled every 2.5 degrees, and look direction is sampled every 5 degrees. This work is still on-going, so for the results in this paper the RCS model in Thompson and Beal (2000) will be used.

The resulting algorithm is totally automated, and can process an entire RADARSAT widescan SAR image in approximately 10 minutes of elapsed time on a multi-user SPARC2 workstation. We believe this is well within the required specifications for an operational system.

3. VALIDATION RESULTS

To validate the performance of the algorithm, 32 RADARSAT SAR images collected off of the east coast of the United States were used. The images contained locations of NOAA buoys which recorded the local wind speed and direction. Some images contained multiple buoy locations and so 52 comparisons were generated. Figure 2 shows an example of the results of the algorithm. The white lines are the SAR-derived wind vectors; the direction represents the wind direction and the length represents the wind speed. The lines have no arrow heads, indicating the 180° ambiguity of the SAR-derived directions. The red lines represent the *in situ* buoy wind vectors that were used for validation. The buoy data was only used if it was located within the image.

Figure 3 shows the results of the wind direction estimation procedure where the SAR-derived wind directions are plotted versus the buoy wind directions. Because of the 180° ambiguity in the SAR-derived directions, they have been resolved to the direction that is closest to the buoy direction. Figure 3 contains a solid line where the points would fall if they were perfect and two dashed lines that indicate the worse possible result (i.e. ±90° from the buoy direction). The stars in Figure 3 represent directions estimate from the SAR image without any spatial smoothing of the wind directions and the solid circles represent the results with spatial smoothing. All the spatial smoothing has done is remove the one significantly errant point toward the left of the plot, although it has dropped the RMSE from 36 ° to 32°. Any wind vector whose ratio of quadratic coefficients were outside of the range mentioned below were eliminated from the test. Without this step the RMSE was 41°. Seven vectors were eliminated with this test, five of which were visually correlated to features not generated by the local wind.

Figure 4 shows the wind speed results. The stars represents estimated wind speed using the algorithm as described here. The resulting RMSE is 4.0 m/s. However one can note a definite trend in Figure 4 where the higher wind speeds are being over estimated. In fact, Figure 5 shows a plot of wind speed error versus the SAR-derived wind speed which indicates a linear trend. This is a bias in the algorithm, perhaps due to calibration errors in the RADARSAT imagery or errors in the RCS model being used. However, since we know the x-axis of Figure 5 (it is the estimated wind speed, not the actual wind speed) we can in fact estimate this bias and remove it as part of the algorithm. The results using this empirical correction are shown in Figure 4 as solid circles. Note that the RMSE is now 1.6 m/s. These results are included in Table1 for comparison.

4. OPERATIONAL IMPLEMENTATION

The algorithm is currently running in a quasi-operational setting as part of the NOAA/NESDIS Alaska SAR Demonstration Project (Pichel and Clemente-Colón, 2000). RADARSAT SAR imagery is acquired by the Alaska SAR Facility over the coast of Alaska, processed into imagery, and sent to the NOAA/NESDIS facility. There, the wind vector algorithm is run automatically whenever imagery arrives and the resulting vectors (both a graphic that overlays the wind vectors onto the SAR image as

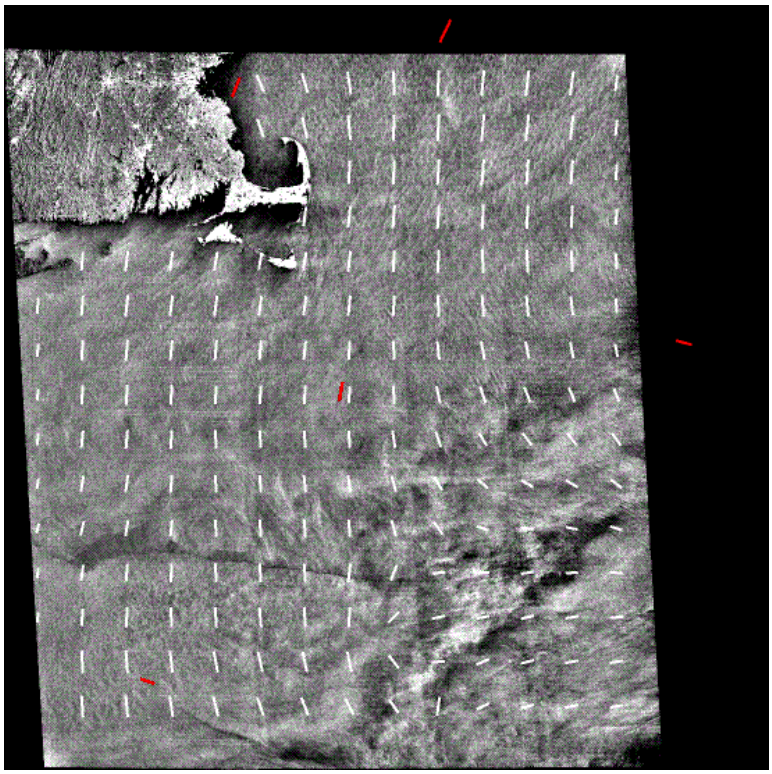

Figure 2: Example results from the wind vector algorithm. SAR-derived vectors are shown in white. Buoy vectors are shown in red. This is for RADARSAT SAR imagery collected 1997, Day 326, Time 223301.

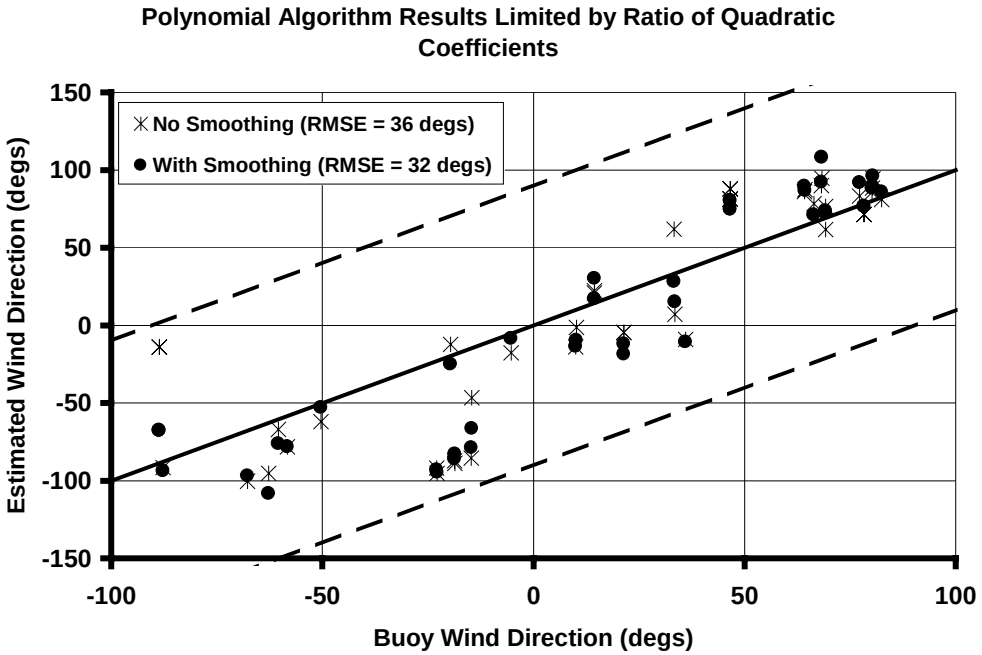

Figure 3: Algorithm performance for estimating wind direction. SAR-derived directions (y-axis) vs. buoy wind directions (x-axis). Solid circles represents results without any spatial smoothing (RMSE = 36 degrees), stars are results after applying the spatial smoothing (RMSE = 32 degrees). Directions which violated the ratio of polynomial coefficients have been removed.

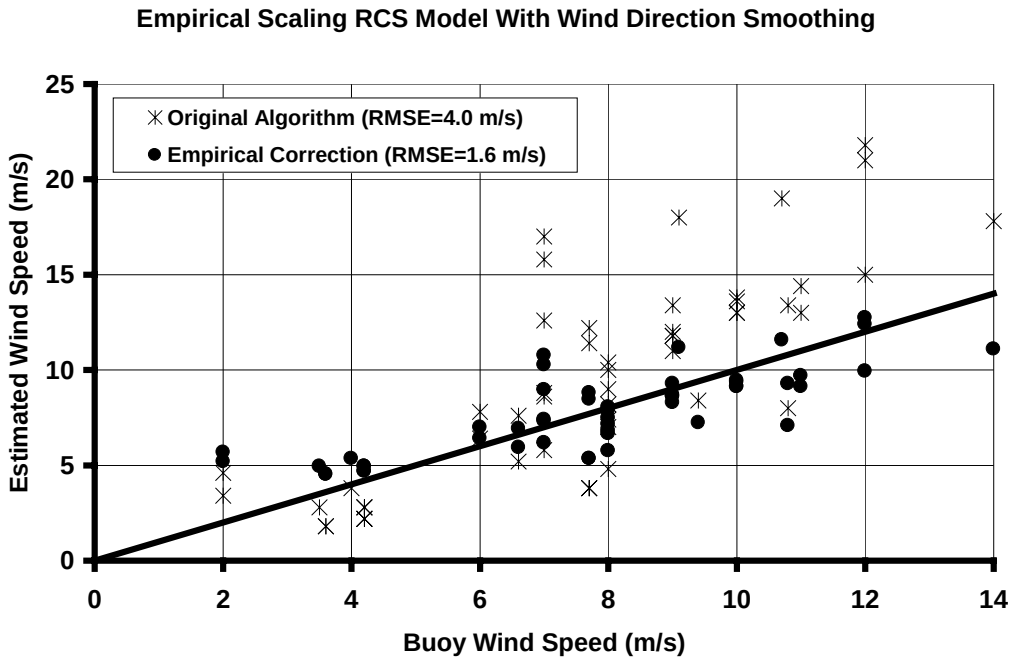

Figure 4: Algorithm performance results for estimating wind speed. SAR-derived wind speeds (y-axis) using SAR-derived wind directions are plotted vs. buoy wind speeds (x-axis). Stars are original algorithm (RMSE = 4.0 m/s) which showed a clear bias with respect to wind speed. Solid circles represents application of the empirical correction (RMSE = 1.6 m/s).

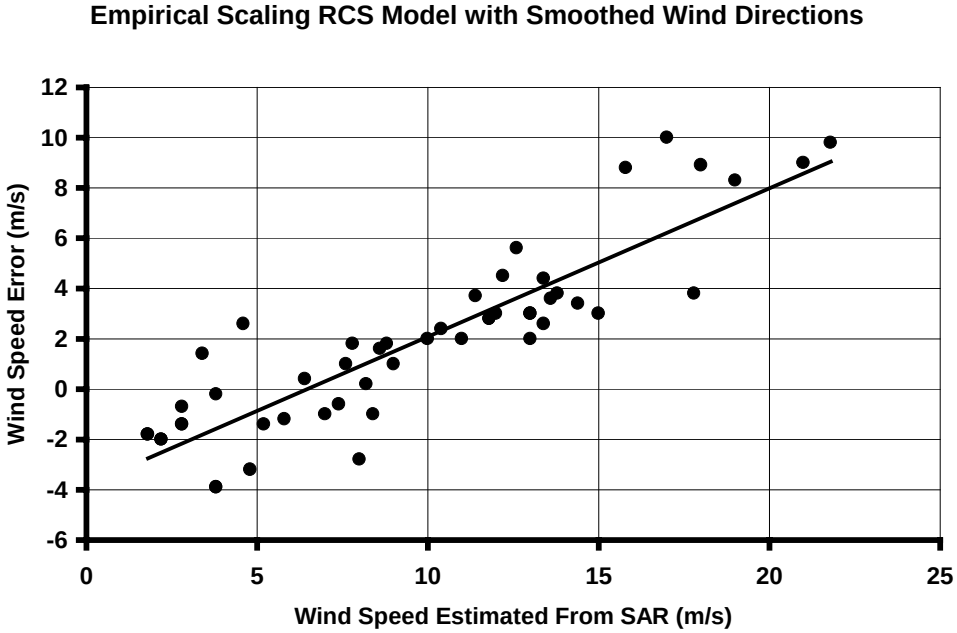

Figure 5: Wind speed error from the original algorithm versus the estimated wind speed. Note the strong linear trend. Since we know the x-axis value (it is the estimated speed not the actual speed) we can correct for the trend.

well as an ascii file that contains the wind vector information) are posted to a password-controlled web site. Users in Alaska can then access the web site to download the wind information. Wind data is available from 5 to 6 hours after acquisition, the delay driven mainly by time to process the SAR data into and image and time to transfer the data. The project has been ongoing for a number of years now and has demonstrated the ability to routinely generate wind vector information from SAR imagery.

5. FUTURE WORK

As mentioned above, work is ongoing to determine whether a better set of metrics exists for automatically eliminating wind directions from local regions and replacing them with either an interpolated direction from the neighboring regions, or some default direction if the SAR image contains no useful direction information. Work is also ongoing to incorporate the analytical RCS model into the wind speed estimation.

6. ACKNOWLEDMENTS

This work was supported by NOAA/NESDIS under Dr. William Pichel and the Office of Naval Research under Dr. Nahid Khazenie. Funding was proved via the Office of Naval Research Contract N00014-00-D-0115-0005.

7. REFERENCES

Du, Y., P. Vachon, J. Wolf, 2002: Wind direction estimation from SAR images of the ocean using wavelet analysis, *Can. J. Remote Sens.*, **28**, 498-509

Fetterer, F., D. Gineris, C. Wackerman, 1998: Validating a scatterometer wind algorithm for ERS-1 SAR. *IEEE Trans. Geosc. Remote Sens.*, **36**, 479-492

Fichaux, N., T. Rachin, 2002: Combined extraction of high spatial resolution wind speed and direction from SAR images: a new approach using wavelet transform, *Can. J. Remote Sens.*, **28**, 510-516

Gerling, T.W. 1986: Structure of the surface wind field from SEASAT SAR, *J. Geophys. Res*., **91**, 2308-2320

Horstmann, J., W. Koch, S. Lehner, R. Tonboe, 2000a: Wind retrieval over the ocean using synthetic aperture radar with C-band HH polarization. . *IEEE Trans. Geosc. Remote Sens.*, **38**, 2122-2131

Horstmann, J., S. Lehner, W. Koch, R. Tonboe, 2000b: Computation of wind vectors over the ocean using spaceborne synthetic aperture radar, *The John Hopkins Univ. Tech. Dig.*, **21**, 100-107.

Horstmann, J., W. Koch, S. Lehner, R. Toeboe, 2002: Ocean winds from RADARSAT-1 ScanSAR, *Can. J. Remote Sens.*, **28**, 524-533

Lehner, S., J. Horstmann, W. Koch, W. Rosenthal, 1998: Mesoscale wind measurements using recalibrated ERS SAR images, *J. Geophys. Res*., **103**,7847-7856

Lehner, S., J. Schulz-Stellenfleth, B. Schattler, H. Breit, J. Horstmann, 2000: Wind and wave measurements using complex ERS-2 SAR wave mode data, *IEEE Trans. Geosc. Remote Sens.*, **38**, 2246-2257

Monaldo, F., 2000: The Alaska SAR demonstration and near-real-time synthetic aperture winds, *The John Hopkins Univ. Tech. Dig.*, **21**, 75-79

Monaldo, F., D.R. Thompson, R.C. Beal, W.G. Pichel, P. Clemente-Colon, 2001: Comparison of SAR-derived wind speed with model predictions and ocean buoy measurements, *IEEE Trans. Geosc. Remote Sens.*, **39**, 2587-2600

Pichel, W.G., P. Clemente-Colon, 2000: NOAA coastwatch SAR applications and demontrations, *The John Hopkins Univ. Tech. Dig.*, **21**, 49-57

Thompson, D.R., R.C. Beal, 2000: Mapping high-resolution wind fields using synthetic aperture radar, *The John Hopkins Univ. Tech. Dig.*, **21**, 58-67

Vachon, P., F.W. Dobson, 1996: Validation of wind vector retrieval from ERS-1 SAR images over the ocean, *Global Atmos. Ocean Syst.*, 177-187

Vachon, P., F.W. Dobson, 2000: Wind retrieval from RADARSAT SAR images: selection of a suitable C-band HH polarization wind retrieval model, *Can. J. Remote Sens.*, **26**, 306-313

Valenzuela, G.R., 1978: Theories for the interaction of electromagnetic and oceanic waves – a review, *Boundary-Layer Meteorology*, **13**, 61-85

Wackerman, C., C.L. Rufenach, R.A. Shuchman, J.A. Johannessen, K.L. Davidson, 1996: Wind vector retrieval using ERS-1 synthetic aperture radar

imagery, *IEEE Trans. Geosc. Remote Sens.*, **34**, 1343-1352

Wackerman, C., P. Clemente-Colon, W. Pichel, X. Li, 2002: A two-scale model to predict C-band VV and HH normalized radar cross section values over the ocean, *Can. J. Remote Sens.*, **28**, 367-384

Wright, J.W., 1968: A new model for sea clutter, *IEEE Trans. Antennas and Propagation.*, **AP-16**, 217-223